Bulletin of the Seismological Society of America, Vol. 88, No. 1, pp. 95–106, February 1998

A Comparison of Select Trigger Algorithms for Automated Global Seismic Phase and Event Detection

by Mitchell Withers*, Richard Aster, Christopher Young, Judy Beiriger, Mark Harris, Susan Moore, and Julian Trujillo

Abstract Digital algorithms for robust detection of phase arrivals in the presence of stationary and nonstationary noise have a long history in seismology and have been exploited primarily to reduce the amount of data recorded by data logging systems to manageable levels. In the present era of inexpensive digital storage, however, such algorithms are increasingly being used to flag signal segments in continuously recorded digital data streams for subsequent processing by automatic and/or expert interpretation systems. In the course of our development of an automated, near-real-time, waveform correlation event-detection and location system (WCEDS), we have surveyed the abilities of such algorithms to enhance seismic phase arrivals in teleseismic data streams. Specifically, we have considered envelopes generated by energy transient (STA/LTA), *Z*-statistic, frequency transient, and polarization algorithms. The WCEDS system requires a set of input data streams that have a smooth, low-amplitude response to background noise and seismic coda and that contain peaks at times corresponding to phase arrivals. The algorithm used to generate these input streams from raw seismograms must perform well under a wide range of source, path, receiver, and noise scenarios. Present computational capabilities allow the application of considerably more robust algorithms than have been historically used in real time. However, highly complex calculations can still be computationally prohibitive for current workstations when the number of data streams become large. While no algorithm was clearly optimal under all source, receiver, path, and noise conditions tested, an STA/LTA algorithm incorporating adaptive window lengths controlled by nonstationary seismogram spectral characteristics was found to provide an output that best met the requirements of a global correlation-based event-detection and location system.

Introduction

Worldwide, approximately 50,000 earthquakes and mining blasts above $m_b \sim 3$ occur annually (e.g., Gutenberg and Richter, 1954), with many thousands exceeding the $m_b = 4.25$ detection threshold goal (e.g., van der Vink *et al.,* 1996) of the International Monitoring System used by the 1996 Comprehensive Test Ban Treaty (CTBT). The considerable investment in human analyst resources necessary to meet the goals of the CTBT as well as the additional interests of the seismological community can be reduced through the application of robust automatic event-detection systems. To this end, we are developing a global waveform correlation event-detection system (WCEDS) at Sandia National Laboratories and New Mexico Tech (Young *et al.,* 1996). It is designed to operate on approximately 150 channels of telemetered broadband data in real time. Conceptually, WCEDS is a pattern-matching, or matched filter, algorithm that detects events by correlating processed seismic data streams with theoretical [e.g., Kenneth and Engdahl (1991), convolved with some envelope function] or empirical (e.g., Shearer, 1991) seismogram envelopes. Phase picks, automatic or otherwise, are not used. A dot product is formed between observed and expected waveforms for lags appropriate for a suite of travel distances that correspond with a geographical grid of epicenters. The output of the WCEDS system consists of a time-dependent correlation value for each grid point considered within the volume of the Earth. High correlation indicates that a seismic signal is present in the data and that the data streams have been properly organized in space and time. Poor correlation either indicates misalignment (improper hypocenter space or time coordi-

*Present address: Center for Earthquake Research and Information, University of Memphis, Memphis, Tennessee 38128.

nates) or the lack of a consistent pattern of seismic phase arrivals in the data. A significant advantage to this methodology is that *a priori* phase identification is not required to identify or locate an event. As correlation with raw waveforms presently would require a prohibitively detailed velocity model and an unmanageable number of free source parameters, the success of the present system is strongly dependent upon our ability to preprocess the data to enhance as many seismic phases as possible in near real time. Many algorithms that can perform this function have previously been developed as triggers to initiate data acquisition. In this article, we restrict our investigation to algorithms, or portions of them, that ideally produce peaks at all constituent phase arrivals and have a smooth and low-amplitude response to seismic background noise and coda. These requirements are governed by the goals of the WCEDS project but are often commensurate with the more generic problem of robust seismic phase and event detection. We organize our investigation into four general categories: time domain, frequency domain, particle motion, and adaptive window length processing.

Previous Work

Time Domain Methods

Freiberger (1963) developed the theory for the maximum likelihood detector assuming Gaussian signal superimposed on Gaussian noise. Unfortunately, real data are not so statistically predictable. Vanderkulk *et al.* (1965) used an STA/LTA algorithm operating on rectified data (e.g., absolute value) because at the time, this allowed significant computational savings over squaring the data.

Allen (1978) developed a detector based on an envelope that is equal to the square of the data plus the weighted square of the first derivative. This creates a time series that includes components of both the unfiltered and high-pass filtered data. The processed data stream is then subjected to a set of logical and mathematical tests for phase identification and timing. Stewart (1977) used a modified data envelope (*MDX*) based on the derivative of the data where slope changes are emphasized. The *MDX* value is found by first estimating the derivative (*DX*) at the *i*th point:

$$DX_i = X_i - X_{i-1}. \tag{1}$$

If the sign of *DX* has been constant for less than eight consecutive *i*, then

$$MDX_i = MDX_{i-1} + DX_i; \tag{2}$$

otherwise,

$$MDX_i = DX_i. \tag{3}$$

The resulting "featherlike" time series is a high-pass realization of the data where the first motion and oscillatory nature of the raw data have been preserved, and emergent signals have been enhanced. A set of detection criteria and thresholds must then be met to declare an event.

Frequency-Domain Methods

Shensa (1977) used the fast Fourier transform to develop a detector based on the power spectral density (PSD). From the PSD, he developed three algorithms: the average power detector, the maximum deflection detector, and the average deflection detector.

The average power detector finds the PSD, $P_i(k)$, at each time step, *i*. The output Y_i, is determined by removing the mean and normalizing by the standard deviation (i.e., "standard normalize") for some frequency index range, $n_1 \leqq k \leqq n_2$.

$$Y_i = \frac{\frac{1}{N}\sum_{k=n_1}^{n_2} P_i(k) - \mu}{\sigma} \quad N = n_2 - n_1, \tag{4}$$

where μ and σ are the mean and standard deviation, respectively, of $P_i(k)$. The average power detector is optimum for weak signals that exceed noise uniformly over a relatively broad range of *k* when both noise and signal are stable.

The maximum deflection detector standard normalizes the PSD at each frequency index, *k*. The maximum value across all frequencies, Z_i, is then output for each time step, *i*.

$$z_i(k) = \frac{P_i(k) - \mu(k)}{\sigma(k)}, \tag{5}$$

$$Z_i = \mathrm{MAX}[z_i(k = 0), z_i(k = 1), \ldots, z_i(k = N)] \tag{6}$$

This detector is optimum for weak signals that exceed noise over at least one narrow frequency band.

The average deflection detector determines the standard normalized PSD for a given frequency index. The output for the *i*th time step, X_i, is the average of this normalized PSD (z_i from 5) across some index range, $n_1 \leqq k \leqq n_2$.

$$X_i = \frac{1}{N}\sum_{k=n_1}^{n_2} z_i(k) \quad N = n_2 - n_1. \tag{7}$$

This detector is optimum on weak signals that exceed background noise uniformly over a relatively wide range of *k* when both signal and noise are unstable.

Because of its speed, Goforth and Herrin (1980) used the Walsh transform (analogous to a Fourier decomposition, except square waves rather than sinusoids are used as basis functions) to generate filter weights in select passbands. Then, as an indicator of nonstationarity, the trigger used a short-term average of the Walsh weights compared to the median and 75th percentile of a long-term set of weights. Masso *et al.* (1979) developed the MARS detector that first applies a suite of bandpass filters to the time series, then

searches each passband for energy peaks. The temporal separation of these peaks is then used to narrow the time window over which to search for the highest-energy nondispersive value, which is then used as the trigger. All of the previously mentioned detectors are reviewed by Berger and Sax (1980), and some are discussed by Allen (1982).

Other Methods

Blandford (1974) used the *F* detector for array data that scans for signals that are coherent, in a slant stack sense, across an array. Anderson (1978) looked for peaks between zero crossings and compared them with a long-term average. An event is declared when the peak exceeds a multiple of the LTA and the associated zero crossings are sufficiently separated. Murdoch and Hutt (1983) developed an efficient algorithm that uses only peaks and troughs along with logical threshold comparisons. Joswig (1990) used a pattern-matching scheme based on the PSD as a function of time. The potential of wavelet transforms applied to seismic data was alluded to by Donoho (1993) and was implemented as a trigger by Ebel (1996). Aster *et al.* (1990), Magotra *et al.* (1987, 1989), Montalbetti and Kanasewich (1970), and Flinn (1965), to name a few, constructed detectors and filters based on the eigenvalues and eigenvectors of the three-component covariance matrix.

To summarize, previous work can be generally categorized into time domain, frequency domain, particle motion processing, or pattern matching. The algorithms discussed so far were often used as triggers for digital data acquisition or for phase identification and timing, ergo they were tuned to detect phase onset. None of the detectors were optimal under all situations, and some were designed to operate under computing systems that are obsolete today. The Allen detector is currently used in many deployments of the widely used Earthworm near real-time network processing system (Johnson *et al.,* 1995) and in the southern California CUSP system (Caltech and USGS Seismic Processing; Dollar, 1989). In combining the energy with the first derivative, the Allen detector incorporates a high-pass filter making it inappropriate for teleseismic data. In the context of the WCEDS waveform correlation, we are primarily interested in generating a suitable data envelope for correlation purposes rather than in detecting phase onset. Following the general time, frequency, particle motion, and adaptive scheme, the output of a few select preprocessing methods will be compared. The preprocessing method used by WCEDS should enhance as many phases as possible with as few preset arbitrary parameters as possible. Further, the processing should have smooth low-amplitude response to background noise and coda (henceforth, just background) and should be computationally parsimonious.

Data

Our data test set consisted of seven different events with between 15 and 35 receivers per event. For brevity, we show results for one event at select receivers. While results vary with source and path, the strengths and weaknesses of the various algorithms can be illustrated by using a variety of seismograms from a single earthquake. The data used were three-component high gain, broadband seismograms obtained from the Global Seismic Network operated by the U.S. Geological Survey and by the Incorporated Research Institutions for Seismology (IRIS). The event shown in all figures is an $m_b \sim 6.2$ earthquake from southern Xinjiang, China, on 2 October 1993 at 08:42:33 UT. Again for brevity, only vertical-component data recorded at station OBN ($\Delta = 38°$) are examined to compare time-domain processing algorithms. Three-component data are used for the remaining frequency, particle motion, and adaptive processing sections. A vertical-component record section for this event is shown in Figure 1 where the time-series amplitudes have been normalized to enhance distant recordings. The travel-time curves are IASPEI 91 (Kennett and Engdahl, 1991).

Time-Domain Processing

The STA/LTA algorithm evaluates the ratio of short- to long-term energy density (squared data). To facilitate combining multi-channel data in a Pythagorean sense, the squared rather than rectified data are used; with current computing capabilities, the additional processing time is trivial. Although optimal window lengths depend on the frequency content of the seismic signal, for IRIS broadband (20 samples/sec) data recorded at teleseismic distances, reasonable body-wave performance can be obtained with window lengths of 3 and 24 sec (Nsta = 60 points and Nlta = 480 points respectively in equations 8 and 9). In our implementation, the short window operates on more recent data than the long window, and there is no overlap or delay; the long-term window begins one data point after the short window, and the time index, i, is set to the most recent point in the STA to preserve causality. We prefer this window placement because it gives better statistical independence between the short- and long-term averages than would overlapping windows. We operate on the vertical-component seismogram shown at the top of Figure 2. The output of the nonrecursive STA/LTA (rectangle impulse response) is shown in Figure 2a, where

$$\mathrm{STA}_i = \frac{x_i^2 - x_{i-N\mathrm{sta}}^2}{N\mathrm{sta}} + \mathrm{STA}_{i-1}, \tag{8}$$

$$\mathrm{LTA}_i = \frac{x_{i-N\mathrm{sta}-1}^2 - x_{i-N\mathrm{sta}-N\mathrm{lta}-1}^2}{N\mathrm{lta}} + \mathrm{LTA}_{i-1}. \tag{9}$$

A better approximation to statistical independence between the two windows can be gained by separating them by a delay time (output shown in Fig. 2b, for delay of 100 samples, Nsta = 60, and Nlta = 480). This method was used by Ruud and Husebye (1992) and is also part of a teleseismic trigger used by L. Powell (personal comm.,

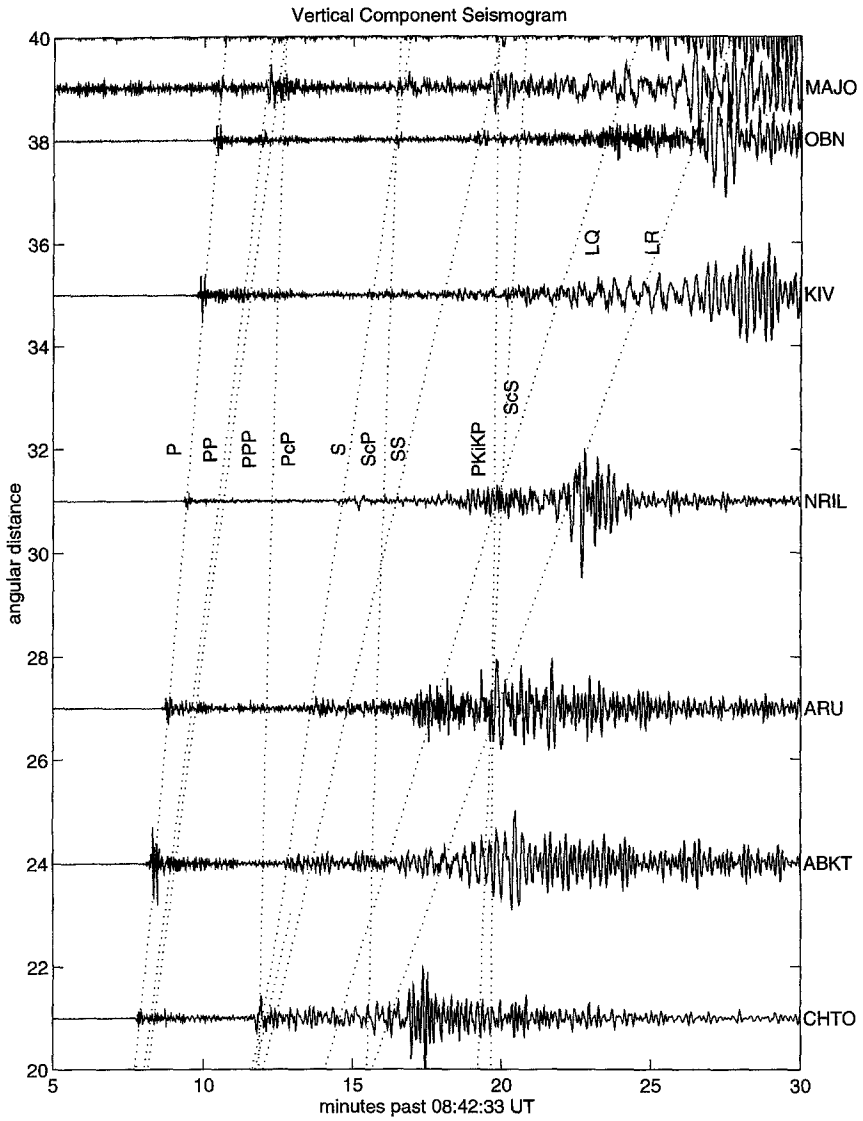

Figure 1. Vertical-component seismograms for an m_b 6.2 earthquake in southern Xinjiang, China, on 2 October 1993 at 08:42:33 UT. Station codes are to the right of the figure. Data are courtesy of IRIS and are positioned vertically to reflect distance between the source and receiver. Traces are amplitude normalized to enhance distant recordings.

1995) in a portable data acquisition system developed at the University of Wisconsin, Madison. The statistical independence of the delayed windows allows shorter window lengths and consequently produces quicker recovery from transients. Shorter windows, however, cause greater variability in the STA/LTA.

It is common to use the recursive STA/LTA to avoid keeping a long data vector in memory. This is more efficient and produces a decaying exponential impulse response, which will recover more quickly from large energy transients, rather than a rectangular impulse response. The recursive scheme also yields smaller "shadow zones" where, after a large transient passes the STA, the transient continues to dominate the output by causing a large LTA. The characteristic decay time, T, is the time required for the impulse response to decay to $1/e$ of its original value (Evans and Allen, 1983) and is embedded in the decay constant, C:

$$\mathrm{STA}_i = Cx_i + (1 - C)\mathrm{STA}_{i-1},$$
$$C = 1 - e^{-S/T}, \tag{10}$$

where S is the seconds per sample and T is the characteristic decay time (it is common to use $C = 1/N\mathrm{sta}$ and $C = 1/N\mathrm{lta}$ for the short- and long-term decay constants). Output for this algorithm is shown in Figure 2c. The effects of the exponential decay are revealed in the smoother response to background. Even though the post-P shadow zone of 2c appears

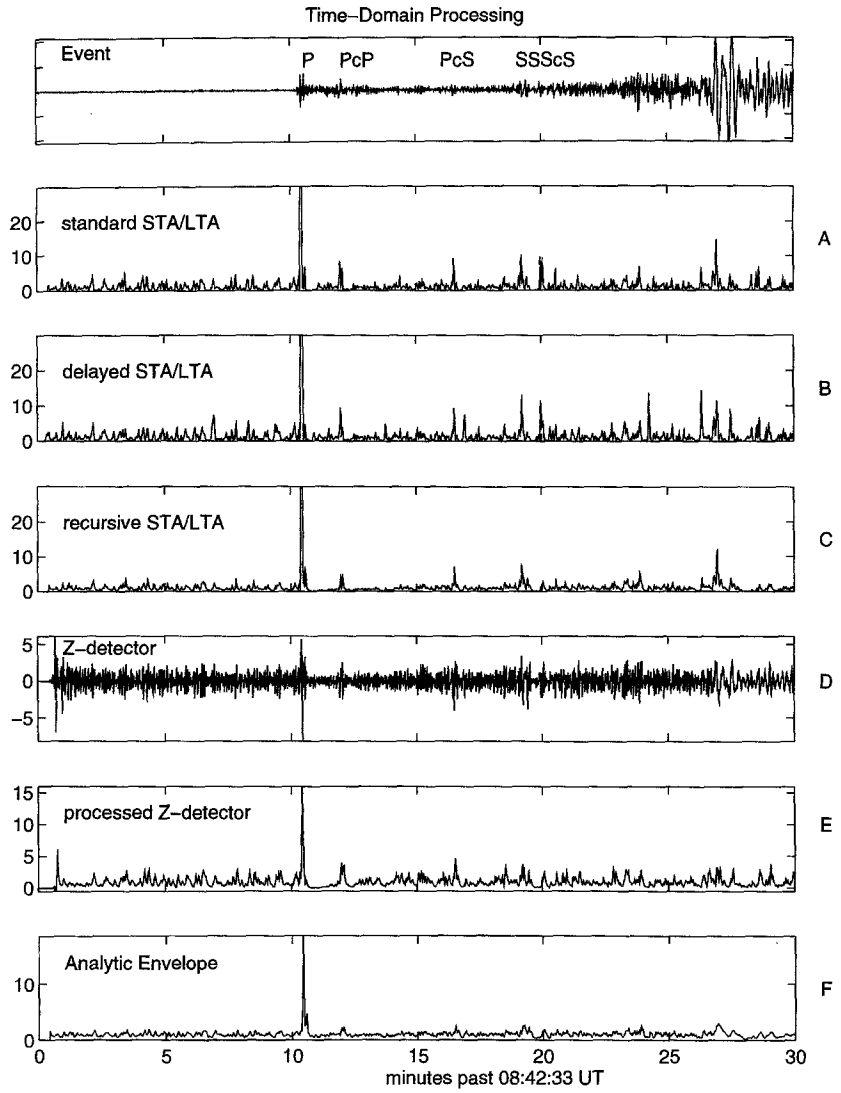

Figure 2. Select time-domain processing methods are shown for the Xinjiang event recorded at GSN station OBN in Obninsk, Russia ($\Delta = 38°$). Algorithms are discussed in the text.

longer than the same zone in 2a, the resolution of this figure is insufficient to adequately display the post-*P* response of the recursive algorithm that is smooth and low amplitude due to the exponential decay in the STA rather than due to the shadow zone.

Swindell and Snell (1977) developed the *Z*-detector, where *Z* is the standardized variable (mean removed, and normalized by the standard deviation).

$$Z(x_i) = \frac{x_i - \mu}{\sigma}. \tag{11}$$

Following the implementation of E. Chael (personal comm., 1995), x is the STA, μ is the average of the STA, and σ is the standard deviation of the STA. The *Z*-detector estimates the distance of the data from the mean in units of the standard deviation. It has the advantage of automatic adjustment to variance in the background noise. If the background variance is small, a small change in input is required for a large change in output. If the background variance is large, a large input change is required for a significant output change. The envelope generated by the *Z*-detector is shown in Figure 2d, but for more direct comparison with other methods, the output of the recursive STA/LTA operating on the *Z*-envelope is shown in Figure 2e. The peak at approximately 1 min in Figure 2d is due to window initialization effects. In this implementation, σ is assumed zero for points prior to the initialization window (2 sec for the STA and 40 sec for the average of the STA) resulting in a very small denominator for the first few points after the 42-sec initialization window. For plotting purposes, the processed data have been decimated with an acausal filter from 20 to 1 samples/sec. This tends to smear the discontinuity at 42 sec into surrounding points resulting in the slight "ramping up" to the initialization peak.

One can also use the analytic envelope (e.g., Earle and Shearer, 1994) rather than the energy as input into the STA/LTA. The analytic envelope is defined as $|x(t) + iH[x(t)]|$ where $H[x(t)]$ is the Hilbert transform and $i = \sqrt{-1}$. The output of the recursive STA/LTA operating on the analytic envelope is shown in Figure 2f.

The nonrecursive and delayed STA/LTA provide peaks at more phases than the other time-domain methods, but their response to background is not as smooth as the recursive STA/LTA and the analytic envelope methods. The *Z*-detector has a noisy response to background and does not enhance secondary arrivals. For the processing methods discussed so far, the recursive STA/LTA appears to provide the best compromise between a smooth low-amplitude response to background and enhances as many phases as possible. Thus, this method is used as a basis for comparison of the next three processing methods discussed in this article. Results for the three-component (channels are squared and summed) records are shown in Figure 3.

Frequency-Domain Processing

The preprocessors discussed previously are detectors of time-domain energy transients. Phase arrivals also introduce transients in the frequency content of the seismogram. To enhance abrupt changes in spectral content, we have developed a frequency-domain nonstationarity (FDN) filter. McGarr *et al.* (1964) used a similar method on windowed *P* arrivals to remove the pre-event noise spectrum from the *P* spectrum.

In this method, PSD estimates are obtained for moving short- and long-term windows positioned much like the STA/LTA windows. Welch's method with 50% overlapping Hann tapers is used to estimate the power spectra in the long-term window and a single Hann taper to obtain the short-term spectral estimate. The long-term spectral magnitude is then subtracted from the short term (and any negative values are set to zero) to generate a difference spectrum.

Using the difference spectrum and the phase from the short-term spectral estimate, the data are then transformed back to the time domain to obtain an FDN filtered data segment. The process is repeated for successive time segments, advancing both windows by the length of the short-term window. To reduce splicing discontinuities, two FDN filtered time series are generated, where the tapers of the second time series are offset from the first by 50% of the short-term window length. The two time series are then summed to obtain a composite output. After FDN filtering, the data are processed with the recursive STA/LTA for direct comparison to other methods. A record section of these outputs is shown in Figure 4.

Some arrivals, such as *S* at NRIL and ARU, have been particularly enhanced by using the FDN filter. The response to background, however, is unacceptably noisy, which is possibly due to poor spectral estimates in the short-term window (a single Hann taper is used in the short-term Welch estimate) and due to the greater sensitivity of the short window, relative to the long window, to high-frequency noise. The short-term PSD estimate may be improved by using multi-taper analysis but not without significant additional processing. One would expect the large-frequency change in surface-wave arrivals to produce large output in the FDN filter. Unfortunately, this filter suffers from the same limitations of many other processing methods, in that a window length must be selected, and this length is usually chosen to be appropriate for body-wave arrivals. In this implementation, a 64-point window (3.2 sec) was used for the short-term spectral estimates. With the 20-Hz sample rate, the first nonzero frequency bin is centered on 0.3125 Hz where, at the distances displayed in the figure, the period of the surface waves will be 20 to 30 sec or more. Longer windows could be used but not without significant additional processing and reduced enhancement of body-wave arrivals.

Particle Motion Processing

A third type of transient that may indicate the arrival of a seismic phase is a change in particle motion. In particular, highly linear particle motion may be associated with body-wave arrivals. To emphasize this feature of the data, the three-component data, (*z, n, e*), are prefiltered with a polarization filter (e.g., Montalbetti and Kanasewich, 1970; Aster *et al.,* 1990). We calculate the data covariance matrix for a moving window (3 sec in this case) and decompose it into matrices of eigenvectors ($\mathbf{U} = [\mathbf{u}_1, \mathbf{u}_2, \mathbf{u}_3]$) and correspondingly sorted nonnegative eigenvalues ($\lambda_1 \geqq \lambda_2 \geqq \lambda_3$). The linearity of the particle motion can then be characterized by a function, *r,* of the eigenvalues, and the direction of linear motion is given by the eigenvector, $\mathbf{u}_1$, associated with the largest eigenvalue, λ_1. The data are then scaled by the linearity vector,

$$\mathbf{r} = \left(1 - \frac{\lambda_2}{\lambda_1}\right)^2 \mathbf{u}_1, \tag{12}$$

to produce a linearity-enhanced seismogram,

$$(z', n', e') = (zr_z, nr_n, er_e). \tag{13}$$

After applying the polarization filter and a Pythagorean summation of the three components, the recursive STA/LTA is applied (Fig. 5). The polarization filtered data have higher peaks at some secondary arrivals than were seen with the unfiltered recursive STA/LTA, and the response to background using the polarization filter is not as noisy as the FDN filtered data. This method is able to produce an output curve with characteristics that are somewhat better for correlation purposes than the unfiltered recursive STA/LTA, but the additional processing involved in diagonalizing the covariance matrix at each time step can be significant.

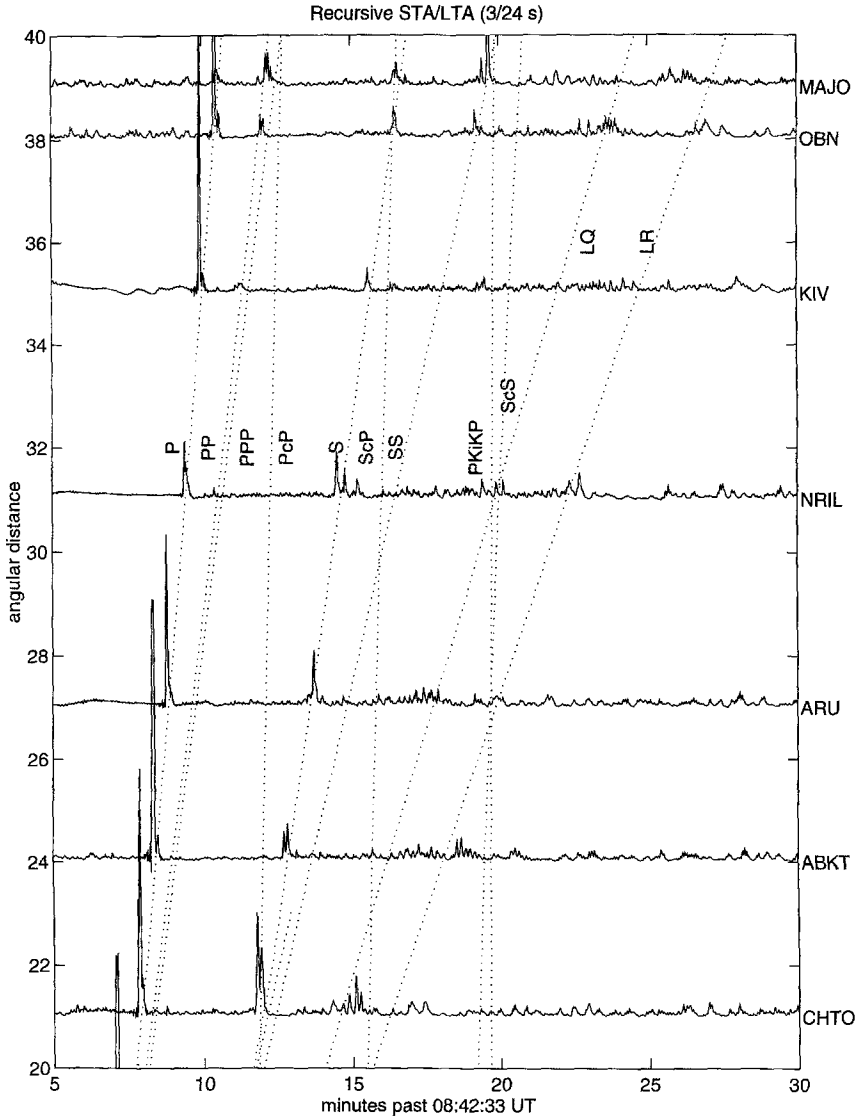

Figure 3. Recursive STA/LTA operating on squared summed three-component data using a 3-sec short-term window and a 24-sec long-term window (see equation 10).

Wagner and Owens (1996) proposed using the frequency-domain principal eigenvalue (λ_1) as a detection statistic, where the covariance matrix is now the dot product of the complex frequency components of each channel. For array data, this provides the advantage of automatic beaming, even for a nonplanar wave front, but a narrow passband must be judiciously chosen, and ray parameter and azimuth information are lost in the dot product. In the limit as the phase lag goes to zero (e.g., three-component single-station data under isotropic path effects) this method reduces to the time-domain eigenvalue decomposition. Care should be taken when comparing statistics that reflect rectilinearity with those that reflect the value of the principal eigenvalue alone. The principal eigenvalue is a measure of the maximum energy in the principal direction that may be quite unrepresentative of the degree of linear particle motion.

Adaptive Processing

The frequency content of a seismogram containing a variety of wave types will vary with time, so adaptively varying the window lengths in the STA/LTA algorithm was investigated. As a fast estimator of the dominant frequency content, the zero crossings are determined in the demeaned data to establish the window length. Requiring six zero crossings in the short-term window (three "cycles") and a long-term window nine times the length of the short-term window provides a reasonable compromise between sensitivity and noise reduction. This strategy was applied to the nonrecursive STA/LTA, operating on the energy. Tong (1995) developed an adaptive STA/LTA that estimates dominant frequency (i.e., segments the data) by requiring that the first derivative be greater than some threshold value. This is a more robust method of estimating the dominant fre-

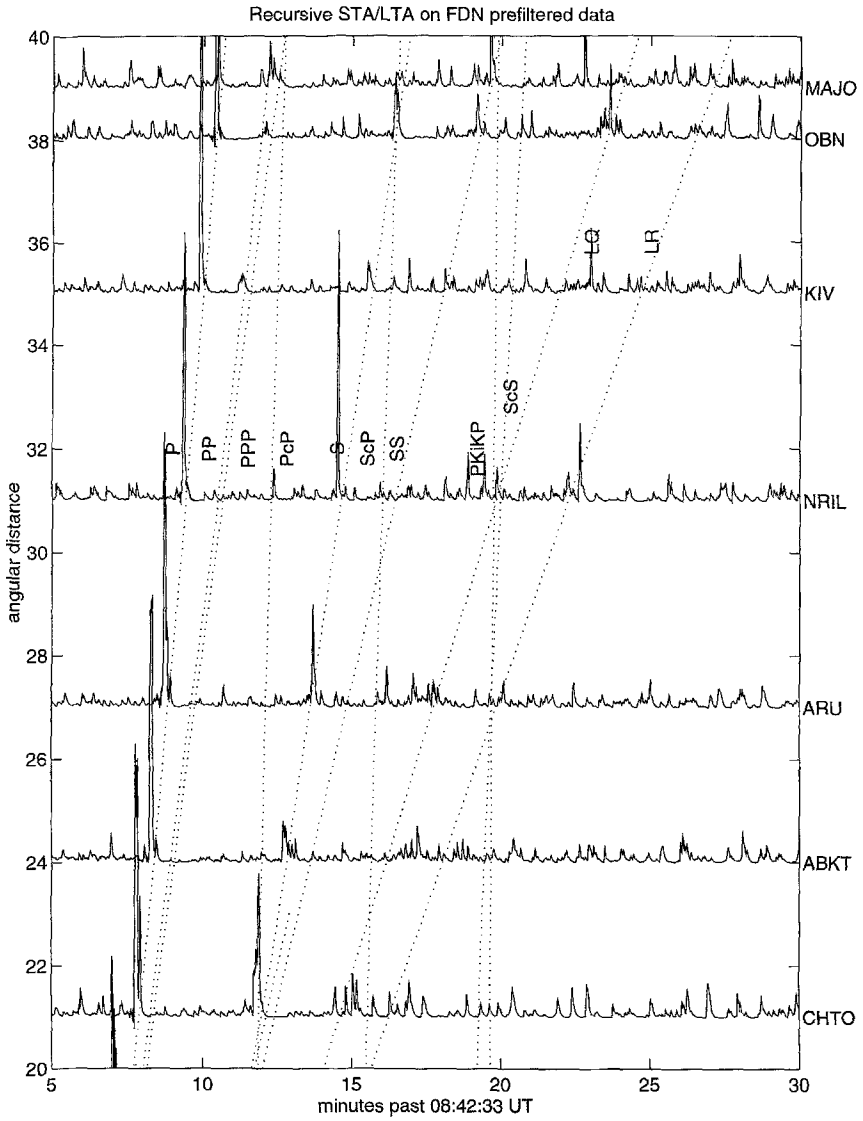

Figure 4. After filtering with the frequency-domain nonstationarity filter, using 3.2 sec (64 points) and 25.6 sec (512 points) for the short and long window lengths, respectively, we process with the recursive STA/LTA. The FDN subtracts the long-term power spectra (noise) from the short-term power spectra (signal).

quency content and does not suffer from the primary disadvantage of the zero-crossing estimation that we have used: low-amplitude short-period arrivals superimposed on high-amplitude long-period arrivals will be missed. Tong uses a recursive STA/LTA and adjusts the window length for a given data segment by changing the decay constant. Implementing the recursive STA/LTA in an adaptive window environment sacrifices sensitivity to phases that have arrival times within the short window length of a previous, higher-frequency arrival because the recursive algorithm requires keeping only the previous average and one data point in memory, and it represents an infinite summation:

$$\mathrm{STA}_i = Cx_i + (1 - C)\mathrm{STA}_{i-1}, \tag{14}$$

$$= Cx_i + C(1 - C)x_{i-1} + C(1 - C)^2x_{i-2} + \cdots. \tag{15}$$

To change the decay constant C requires resumming the data. One might be tempted to apply the new decay constant beginning at the ith point, but this presents the possibility of generating a very poor estimate. This is particularly true for the LTA in an expanding window. In such a case, the new "longer-period" LTA will be unjustifiably large because the appropriate new decay constant should be small (but cannot be made so without resumming the data) relative to the old, shorter window constant. Applying a nonrecursive algorithm in an adaptive window length environment thus preserves the correct relative contributions of the short and long windows based on the dominant frequency of the current data points at the expense of the exponential decay of the recursive procedure. On the other hand, applying the recursive

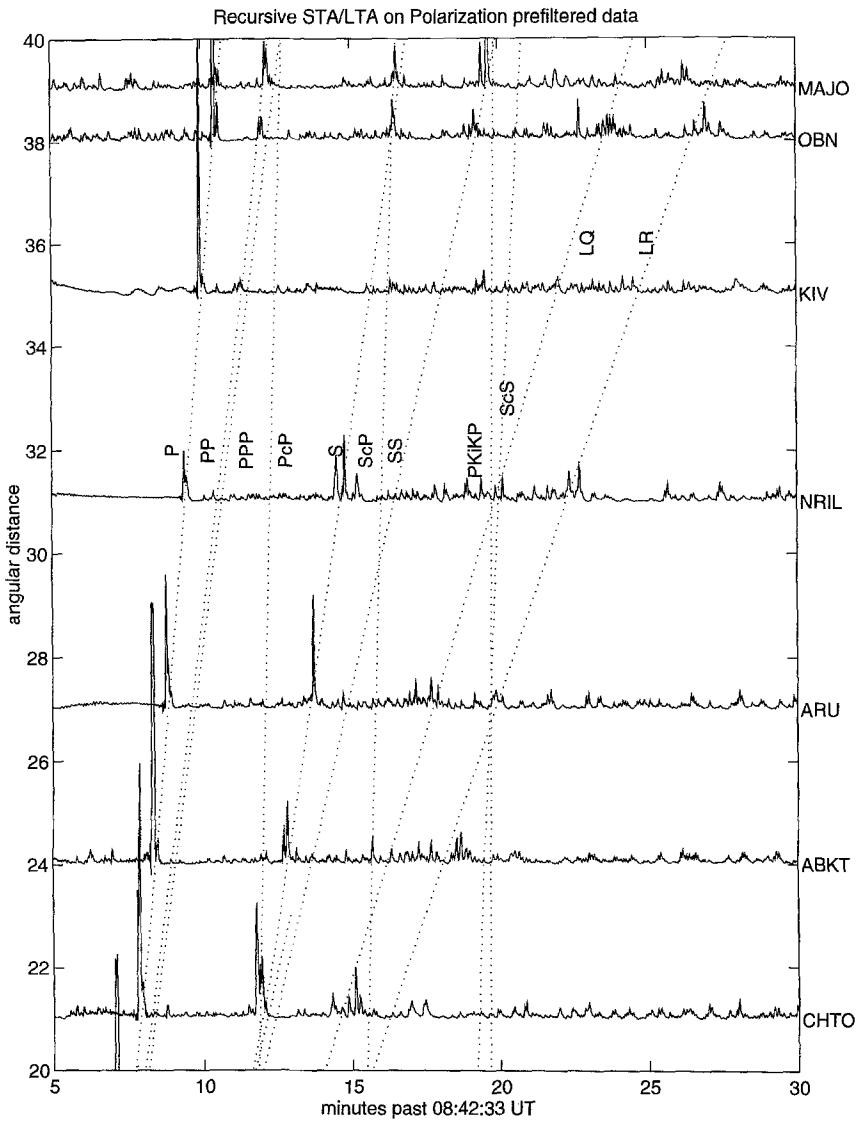

Figure 5. After filtering for linear particle motion using a 3-sec moving window, the data are processed with the recursive STA/LTA. The filter applies weights to the time-domain data, where the weights are related to the eigenvalues and eigenvectors of the decomposed covariance matrix.

algorithm in the adaptive environment sacrifices sensitivity to closely spaced arrivals with decreasing dominant frequency but retains the advantages of exponential decay in the impulse response. We have opted to sacrifice memory and the exponential decay by using the nonrecursive STA/LTA so that we retain sensitivity to closely spaced arrivals with significantly different dominant frequencies. Because the windows are usually short, there is very little penalty in not incorporating the exponential decay, and processing time is not significantly affected. For large data sets, memory use could become significant.

Low-frequency signals (e.g., surface waves) may produce extremely broad peaks in the output of the adaptive STA/LTA that could mask other, shorter-period arrivals. We mitigate this effect by capping the short window length at 60 sec. Within the limitation imposed by this clamp, windows may expand within the seismic coda as they generally encounter longer-period arrivals. When the LTA expands backward into a previous large arrival (e.g., into *P* while operating on *PcP*), the previous arrival may significantly perturb the long-term average and thus adversely bias the desired output peak corresponding to the later arrival (i.e., create a shadow zone). To control this effect, the additional data to be added into the back-expanding long-term window is examined. If the power in the new long-term window segment is greater than 10 times that of a similar-length average piece of the previous long-term window (indicative of a large energy transient), the STA/LTA calculation instead uses the appropriate fraction of the previous LTA energy rather than the data itself (not unlike the recursive realization where

$C = 1/N\text{lta}$). The output of the adaptive STA/LTA is shown in the gather in Figure 6.

This algorithm produces large peaks at most arrivals and has smooth, low amplitude response to background. Further, the method need not be tuned to a given frequency band and is able to enhance both short- and long-period arrivals with a single algorithm. The resulting processed waveform is a clearer representation of the data envelope than that generated by other methods and is thus more suitable for correlation. Only very small increases in memory use and processing time are required over the recursive STA/LTA. An additional data stream (zero crossings) for each station is incorporated, but these may be determined "on the fly." The zero-crossing method of estimating dominant frequency may cause short-period phases to be obscured if they are superimposed on long-period coda.

Discussion and Summary

Significant gains in computing capabilities have allowed more sophisticated processing algorithms to operate in real time. Even with these gains, however, the more processing intensive methods may still be overwhelmed when many data channels must be processed simultaneously. Philosophically, we prefer simplicity and consequently demand that more complex methods provide greater return. Because the data are time series, time-domain methods are, in general, less complex.

The nonrecursive STA/LTA has a rectangular impulse response, and performance can be enhanced by using squared data (energy) rather than rectified data. The difference in processing time between squaring and rectifying, although once a significant concern, is negligible on modern

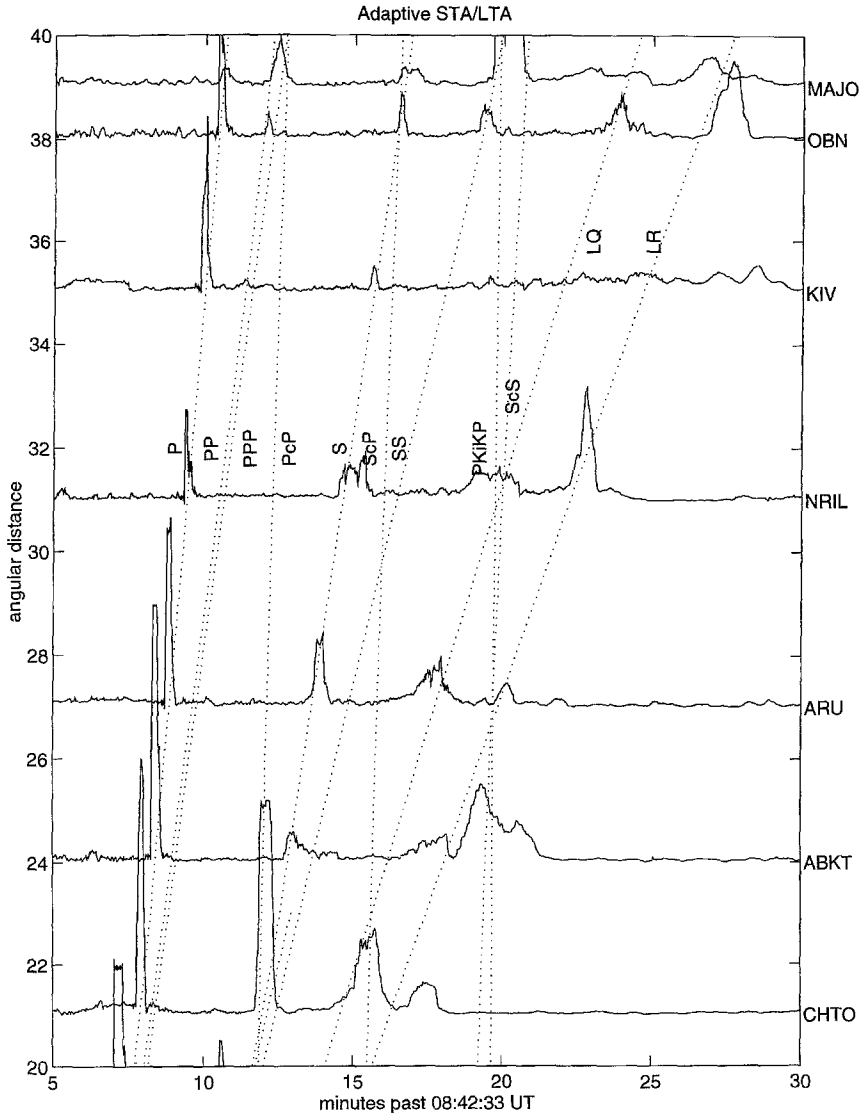

Figure 6. The adaptive STA/LTA has window lengths that are updated at every point such that the short-term window (within the bounds of minimum and maximum lengths of 0.6 and 60 sec, respectively) contains six zero crossings. The long-term window is nine times the length of the short-term window.

computers. To more closely approximate statistical independence between the STA and LTA windows, no overlap between the two windows is permitted. To maintain causality, the time index is fixed to the first point of the STA. Statistical independence can be further improved by separating the windows by some delay time. This allows shorter windows and consequently shorter shadow zones caused by energy transient saturation of the LTA. We can further reduce transient effects and significantly reduce computer memory requirements by using the recursive algorithm that has an exponentially decaying impulse response.

A bank of bandpass filters has often been used to prefilter the data prior to generating the data envelope. This is particularly useful for separating phases that have significantly different path lengths and for triggering on high-frequency local events superimposed on teleseismic coda or long-period noise. The real-time performance of a system with many stations, however, may be deleteriously affected by the additional channels. We have developed a "noise" subtracting FDN filter in an attempt to consider the wide range of frequency bands encompassed by the suite of possible phase arrivals without adding additional data streams, but the smoothness of this algorithm in the presence of real background noise is less than satisfying. Better signal spectra could be estimated for the FDN filter if multi-taper analysis (Park *et al.,* 1987) were used (currently the short-term spectra are estimated with a single Hann taper), but this would be computationally expensive as multiple-spectral estimates would have to be generated at each time step.

One can also search for linear particle motion in detecting body-wave phases, but near-surface scattering and superimposed wind-generated seismic background noise can have a significant corroding influence on linearity (Withers *et al.,* 1996). Furthermore, for the window lengths used, some background noise sources may generate particle motion with significant linearity.

Because frequency-domain and particle-motion methods are generally more computationally intensive than time-domain methods, processing requirements are significantly greater. These requirements may be mitigated with larger time steps at the expense of resolution. If numerous data streams must be processed in real time, the added complexity may not be justified by the relatively minor gains in the data envelope.

Nearly any algorithm may be enhanced by implementing an adaptive window. The time-domain and particle-motion methods suffer from tuning the windows to *P* arrivals. Even the attempt to adaptively filter the time series using the frequency-domain noise-subtracting method of the FDN filter failed to enhance surface-wave arrivals because the window lengths used for the spectral estimates were tuned to body-wave arrivals. If the windows were expanded to include sufficient resolution to enhance surface waves, the number of points in the fast Fourier transform would require prohibitive processing.

For the adaptive STA/LTA, we have based our window length on a crude estimate of the dominant frequency that might be improved by using a more robust technique (e.g., Tong, 1995). Better window length adjustment may become particularly useful in the case where a local event is superimposed on teleseismic surface waves. Our current technique might "miss" the local event since the window length would be dominated by the surface wave.

Conclusions

An optimal data envelope is required for input into the WCEDS correlation. Thus, less importance is placed on triggers and phase identification than in producing high signal-to-noise peaks at as many phases as possible without producing an appreciable number of spurious peaks. The *Z*-detector, for example, may do well as a trigger, but the envelope it generates is suboptimal for correlation with synthetic envelopes because of a relatively high noise level. We have also found that squaring the data is preferable to rectifying. The recursive STA/LTA provides reduced memory requirements and is smoother in the absence of signal. Gains from the FDN and Polarization filters were not worth the orders of magnitude greater processing, nor did they consistently perform as well as the adaptive STA/LTA. Not surprisingly, no specific algorithm and set of user-defined parameters is optimal for all scenarios of source, path, receiver, and background noise. Nearly any processing technique that requires windowing will benefit from adaptively updating the window length; the polarization filter, for example, would benefit from having a longer correlation window in background noise and a shorter window during seismic phase arrivals. While not without disadvantages (such as "missed" high-frequency phases that are superimposed on higher-amplitude, longer-period phases), the adaptive STA/LTA algorithm is able to enhance phases over a broad frequency band with a single algorithm.

The Waveform Correlation Event Detection System will use the adaptive STA/LTA for its ability to enhance phase arrivals over a wide range of source, path, receiver, and noise scenarios with a single algorithm. This will become more important as the magnitude threshold is reduced because surface-wave arrivals are often the only discernible phases for small shallow events at regional and teleseismic distances.

Acknowledgments

We greatly appreciate the assistance of Bob Hutt and Jim Murdoch of the Albuquerque Seismic Lab and Eric Chael at Sandia. This article was improved by a comprehensive review from Marianne Walck at Sandia Labs. This work was supported by the U.S. Department of Energy under Contract Number DE-AC04-94-AL85000. Sandia is a multi-program laboratory operated by Sandia Corporation, a Lockheed Martin Company, for the U.S. Department of Energy. This is CERI Contribution Number 345.

References

Allen, R. (1978). Automatic earthquake recognition and timing from single traces, *Bull. Seism. Soc. Am.* **68,** 1521–1532.

Allen, R. (1982). Automatic phase pickers: their present use and future prospects, *Bull. Seism. Soc. Am.* **72,** S225–S242.

Anderson, K. (1978). Automatic analysis of microearthquake data, *Geoexploration* **16,** 159–175.

Aster, R., P. Shearer, and J. Berger (1990). Quantitative measurements of shear wave polarizations at the Anza seismic network, southern California: implications for shear wave splitting and earthquake prediction, *J. Geophys. Res.* **95,** 12449–12473.

Berger, J. and R. Sax (1980). Seismic detectors: the state of the art, AFTAC unclassified report, SSS-R-80-4588, 103 pp.

Blandford, R. (1974). An automatic event detector at the Tonto Forest seismic observatory, *Geophysics* **39,** 633–643.

Dollar, R. (1989). Realtime CUSP: automated earthquake detection system for large networks, *U.S. Geol. Surv. Open-File Rept. 89-320,* 3 pp.

Donoho, D. (1993). Nonlinear wavelet methods for recovery of signals, densities, and spectra from indirect and noisy data, *Proc. of Symp. Appl. Math.* **47,** 173–205.

Earle, P. and P. Shearer (1994). Characterization of global seismograms using an automatic-picking algorithm, *Bull. Seism. Soc. Am.* **84,** 366–376.

Ebel, J. (1996). Development of a seismic event detection and identification algorithm based on wavelet transforms, *Seism. Res. Lett.* **67,** no. 2, 37.

Evans, J. and S. Allen (1983). A teleseismic-specific detection algorithm for single short period traces, *Bull. Seism. Soc. Am.* **73,** 1173–1186.

Flinn, E. (1965). Signal analysis using rectilinearity and direction of particle motion, *Proc. IEEE* **53,** 1874–1876.

Freiberger, W. (1963). An approximate method in signal detection, *J. Appl. Math.* **20,** 373–378.

Goforth, T. and E. Herrin (1981). An automatic seismic signal detection algorithm based on the Walsh transform, *Bull. Seism. Soc. Am.* **71,** 1351–1360.

Gutenberg, B. and C. Richter (1954). *Seismicity of the Earth and Associated Phenomena,* Princeton Univ. Press, Princeton.

Johnson, C., A. Bittenbinder, B. Bogaert, L. Dietz, and W. Kohler (1995). Earthworm: a flexible approach to seismic network processing, *IRIS Newslett.* **14,** no. 2, 1–4.

Joswig, M. (1990). Pattern recognition for earthquake detection, *Bull. Seism. Soc. Am.* **80,** 170–186.

Kennett, B. and E. Engdahl (1991). Traveltimes for global earthquake location and phase identification, *Geophys. J. Int.* **105,** 429–465.

Magotra, N., N. Ahmed, and E. Chael (1987). Seismic event detection and source location using single-station (three-component) data, *Bull. Seism. Soc. Am.* **77,** 958–971.

Magotra, N., N. Ahmed, and E. Chael (1989). Single-station seismic event detection and location, *IEEE Trans. Geosci. Remote Sensing* **27,** 15–23.

Masso, J., C. Archambeau, and J. Savino (1979). Implementation, testing, and specification of a seismic event detection and discrimination system, Systems, Science, and Software Report, SSS-R-79-3963.

McGarr, A., R. Hofmann, and G. Hair (1964). A moving-time-window signal-spectra process, *Geophysics* **29,** 212–220.

Montalbetti, J. and E. Kanasewich (1970). Enhancement of teleseismic body phases with a polarization filter, *Geophys. J. R. Astr. Soc.* **21,** 119–129.

Murdoch, J. and C. Hutt (1983). A new event detector designed for the seismic research observatories, *U.S. Geol. Surv. Open-File Rep. 83-785,* 37 pp.

Park, J., C. Lindberg, and F. Vernon (1987). Multitaper spectral analysis of high-frequency seismograms, *J. Geophys. Res.* **92,** 12675–12684.

Ruud, B. and E. Husebye (1992). A new three-component detector and automatic single-station bulletin production, *Bull. Seism. Soc. Am.* **82,** 221–237.

Shearer, Peter M. (1991). Imaging global body wave phases by stacking long-period seismograms, *J. Geophys. Res.* **96,** 20353–20364.

Shensa, M. (1977). The deflection detector, its theory and evaluation on short-period seismic data, TR-77-03, Texas Instruments, Alexandria, Virginia.

Stewart, S. (1977). Real-time detection and location of local seismic events in central California, *Bull. Seism. Soc. Am.* **67,** 433–452.

Swindell, H., and N. Snell (1977). Station processor automatic signal detection system, phase I: final report, station processor software development, Texas Instruments Report No. ALEX (01)-FR-77-01.

Tong, Chen (1995). Characterization of seismic phases-an automatic analyser for seismograms, *Geophys. J. Int.* **123,** 937–947.

Vanderkulk, W., F. Rosen, and S. Lorenz (1965). Large aperture seismic array signal processing study, IBM Final Report, ARPA Contract Number SD-296.

van der Vink, G., D. Simpson, R. Butler, C. Hennet, and T. Wallace (1996). CTBT . . . at last! *IRIS Newslett.* **XV,** no. 3, 1–3.

Wagner, G. and T. Owens (1996). Signal detection using multi-channel seismic data, *Bull. Seism. Soc. Am.* **86,** 221–231.

Withers, M., R. Aster, C. Young, and E. Chael (1996). High-frequency analysis of seismic background noise as a function of wind speed and shallow depth, *Bull. Seism. Soc. Am.* **86,** 1507–1515.

Young, C., J. Beiriger, M. Harris, S. Moore, J. Trujillo, M. Withers, and R. Aster (1996). The waveform correlation event detection system project phase I: issues in prototype development and testing, Internal Report, Department of Energy, Office of Research and Development, NN20, 45 pp.

Department of Earth and Environmental Science and Geophysical Research Center
New Mexico Institute of Mining and Technology
Socorro, New Mexico 87801
(M.W., R.A.)

Sandia National Laboratories
Albuquerque, New Mexico 87185
(C.Y., J.B., M.H., S.M., J.T.)

Manuscript received 21 April 1997.